

Interactions of RF Antennas with the Edge Plasma in Tore Supra Steady-State Discharges

M.Goniche 1), L.Colas 1), A.Ekedahl 1), M.Chantant 1), V. Petržílka 2), V.Basiuk 1), Ph.Bibet 1), L.Delpech 1), L.-G.Eriksson 1), J.Gunn 1), S.Heuraux 3), E.Joffrin 1), F.Kazarian 1), G.Lombard 1), C.Lowry 1), L.Millon 1), P.Mollard 1), P.Moreau 1), C.Portafaix 1), M.Prou 1), H.Roche 1), J.M.Travère 1)

1) Association EURATOM-CEA sur la Fusion, DSM/Département de Recherches sur la Fusion Contrôlée, CEA-Cadarache, 13108 Saint Paul-lez-Durance, France

2) Association EURATOM/IPP.CR, Prague, Czech Republic

3) LPMIA, UMR 7040 CNRS, BP 239 F-54506 Vandoeuvre cedex, France

e-mail contact of main author: marc.goniche@cea.fr

Abstract. Specific phenomena arising in the vicinity of antennas operating in the Ion Cyclotron Range of Frequency (ICRF) or the Lower Hybrid Range of Frequency (LHRF) are identified on the Tore Supra tokamak. The involved mechanisms have to be investigated in order to ensure safe and controlled operation in future fusion devices. These phenomena break the symmetry of the unperturbed scrape-off layer and 2D diagnostics are needed to address this topic.

This study is mainly based on measurements provided by the infra-red (IR) imaging diagnostic and the Langmuir probes. The powerful IR diagnostic which monitors the total area of the three ICRF antennas and two LHRF launchers allows a detailed analysis of the heat flux deposition in steady-state condition with a good spatial resolution (~1cm). 2D mapping of the plasma layer in the vicinity of an ICRF antenna has been performed with a reciprocating probe by scanning the radial position of the probe and the field line tilt for poloidal resolution.. These data are complemented by calorimetric measurements of the energy extracted by the cooling loops on the antennas and their side limiters. A large database of these global measurements allows to estimate the power lost by each specific phenomena and scaling laws are proposed for a LH launcher and an ICRF antenna.

This identification of heat flux deposition sources has been integrated in the real-time control system of Tore Supra in order to optimize the RF power output without deleterious effects. In such conditions discharges with 9.5MW for 23s have been successfully achieved

1.Introduction

High frequency antennas operating in the Ion Cyclotron Range of Frequency (ICRF) or the Lower Hybrid Range of Frequency (LHRF) are exposed to heat flux deposition from the plasma. In order to reduce this heat flux, the gap between the plasma and the last closed flux surface (LCFS) has to be as large as possible but compatible with good wave coupling. In ITER it is planned to have the front of the antennas aligned with the beryllium-covered wall. Although this should guarantee low enough heat flux from the convected/conducted power, specific phenomena arising from the intense oscillating electric field in front of the antennas, leading to the acceleration of ions and/or electrons, are up to now not fully taken into account. The involved mechanisms have to be investigated in order to ensure safe and controlled operation in future fusion devices.

2.RF systems and diagnostics

On Tore Supra, 3 ICRF antennas and 2 LHRF launchers, installed in separate equatorial ports, provide high power capabilities for plasma heating and current drive. The ICRF antennas (Q1, Q2 and Q5) consists of two radiating straps embedded in a metallic box, partially closed on the plasma side by a tilted B₄C-covered Faraday screen. The LHRF launchers C2 and C3 are composed of 4 and 6 rows, respectively, of 32 active copper-alloy waveguides poloidally

stacked. For the ICRF antennas, antisymmetric strap phasing $(0, \pi)$ is used in D(H) minority heating at the RF frequency of 57MHz and $\pi/2$ phasing of the LHRF waveguides provides the low parallel refractive index ($n_{\parallel} \approx 1.85$) for current drive at 3.7GHz. The launchers are slightly retracted with respect of the ICRH antennas by 1-2cm when the two systems are combined. Because of the toroidal location of these components, the LH launchers are shadowed by the Q1 and Q5 antennas. Moreover, each component is shadowed by two private CFC limiters which are protruding with respect to the Faraday screen by 4mm (edge) to 13mm (center) and to the waveguides by only 1.5mm.

The total area of the ICRF antennas and LHRF launchers are monitored by an infrared (IR) system [1]. The good spatial resolution (~ 1 cm) of this diagnostic allow identifying specific phenomena of plasma-antenna interaction. The IR data are complemented by calorimetric measurements of the energy extracted by the cooling loops on each antenna and their side limiters. The long pulse capability of Tore Supra allows to assess plasma-antenna interaction in steady state plasmas. Whereas the time constant of the ICRH antennas is of the order of 10s, stationary conditions of the LH launchers require pulse lengths of ~ 200 s to achieve thermal equilibrium. Both fixed Langmuir probes (LP) embedded in the LH launchers and reciprocating probes, which can be magnetically connected to the RF antennas, are used for studying the local electric potential and electron density perturbation. In particular a detailed 2D mapping of the scrape-off layer perturbation in the vicinity of an ICRF antenna has been performed for the first time, using a reciprocating double probe.

3.ICRF-induced SOL perturbations

In the ICRF regime, RF sheath rectification can raise locally the plasma potential up to several hundreds eV [2]. Stochastic electron acceleration in the ICRF parallel near field could also bias the edge flux tubes positively [3]. In both cases ions accelerated across the enhanced DC sheath potentials increase the heat loads onto antenna front faces. Besides, differential biasing of nearby flux tubes creates DC $\mathbf{E} \times \mathbf{B}$ flows, presently directed upwards on Tore Supra. Poloidal density inhomogeneity, expected from this $\mathbf{E} \times \mathbf{B}$ convection, is also suspected from IR images of powered antennas : upper-left box corners appear systematically hotter than lower-right ones (figure 1). This hot spot asymmetry is attributed to density unbalance and was reversed when the magnetic field was inverted.

For the first time a 2D mapping of the SOL perturbation in the flux tubes passing in the vicinity of the antenna has been performed with a reciprocating Langmuir probe [5]. Radial resolution is provided by the probe reciprocation while poloidal resolution is provided by scanning the edge safety factor through plasma current steps. The antenna point connected to the probe is labeled by its altitude Z with respect to the equatorial plane and its radial distance δr to the side limiters leading edge. From shot to shot several ICRF antennas were combined for four private power levels (0, 0.5, 1, 1.5MW). 950 kW of LHRF power was added for coupling measurements.

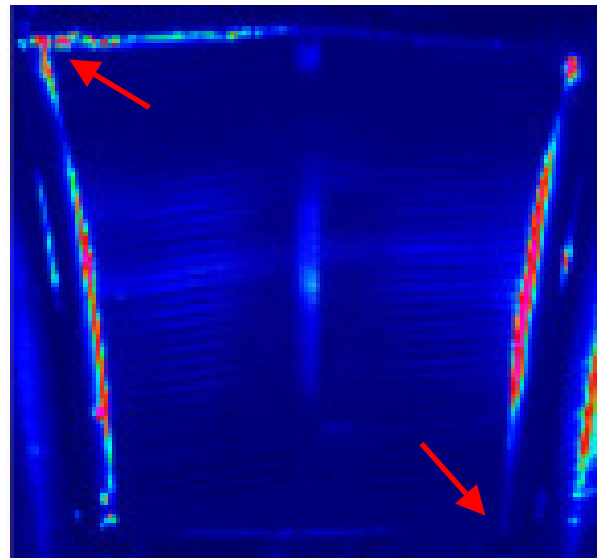


Figure1. IR image of an ICRF antenna (#37843 - $P_{Q5} = 2MW$)

The floating potential which is the potential when no current flows into the probe is first investigated. V_{float} differs from the plasma potential V_p by $V_p - V_{\text{float}} \sim 3T_e$ for a thermal plasma. When the antenna Q5 is passive, V_{float} is slightly negative and slowly increases radially outwards. When the antenna Q5 is powered, a high positive peaks appears on the connected side of the probe and the other probe, un-connected, shows no modification. The roles of the two probes are exchanged when antenna Q5 is left passive and antenna Q1 is powered. The radial zone of the ICRH-perturbed zone is radially centered near the leading edge of the side limiters and has a typical radial width of 2cm (figure 2). This is only a few times larger than electrodes dimensions (diameter 4mm) and instrumental broadening is not excluded. The ICRF power level has unexpectedly a very weak effect and the power dependence of the V_{float} maximum is much less than the $P^{1/2}$ dependence observed for the antenna front face temperature [6]. At high power, an unexplained two-peak structure seems to emerge, particularly for high $|Z|$. Poloidal scan of V_{float} shows also strong variations when the antenna is powered. A local minimum is observed near $Z=0$ and local maxima near lower and upper parts of the antenna box (figure 3). A similar pattern is obtained for the electron temperature (T_e) and it should be noted that the zones of high T_e coincides with those of high potential

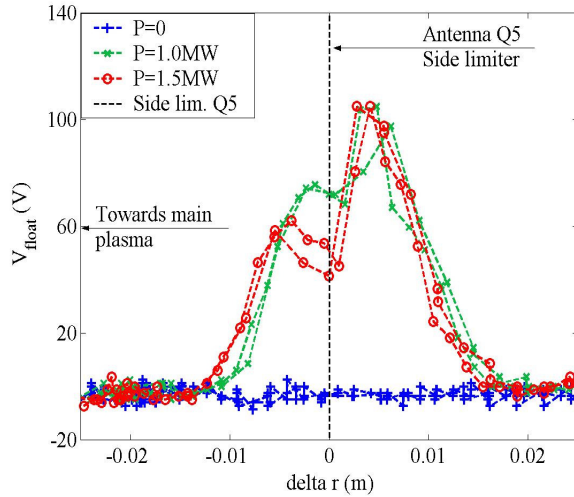


Figure 2. Floating potential as a function of δr for 3 RF powers (0, 1 and 1.5MW) and $I_p=1.2MA$ (Q5 antenna).

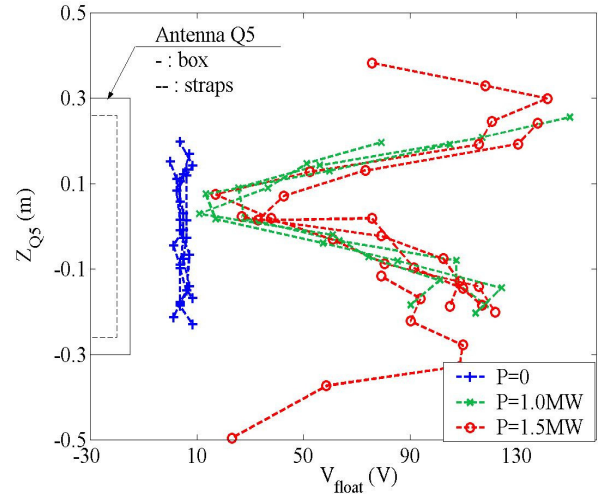


Figure 3. Floating potential as a function of Z for 3 RF powers (0,1 and 1.5MW) at local radial maxima

V_{float} was also measured as a function of the confined plasma density. When the line-averaged density increases from $\bar{n} = 2.75 \times 10^{19} \text{m}^{-3}$ to $4.05 \times 10^{19} \text{m}^{-3}$ during a 14-second ramp, the maximum of V_{float} strongly decreases from $\sim 130\text{V}$ to $\sim 30\text{V}$. At the same time the coupling resistance increases from $2.8 \Omega/\text{m}$ to $6.3 \Omega/\text{m}$ (figure 4). It should be noted that V_{float} decreases mostly at the beginning of the density ramp whereas the coupling is almost unchanged. This could be the result of the density response to the strong gas injection ($1.5\text{--}2.5 \text{Pa}\cdot\text{m}^3/\text{s}$) performed for rising the density. When the density increases the coupling improves and the RF electric field, for a constant coupled power, decreases. As a consequence a reduction of V_{float} is expected. There is an other mechanism which leads to the reduction of V_{float} . The skin depth of the slow wave c/ω_{pe} decreases when density increases and therefore the slow wave, responsible of the parallel electric field, is more efficiently damped.

The probe saturation current I_{sat} , which is representative of the local plasma density if saturation is effectively achieved, is also obtained from the same shots. To eliminate global effects of the plasma current and additional power on the whole SOL, I_{sat} is normalized to the value in the unperturbed zone at $\delta r = -0.025\text{m}$. On figure 5, normalized I_{sat} is mapped as a function of $(\delta r, Z)$ for $P=1.5\text{MW}$. When the antenna is passive, such map is poloidally homogeneous and exhibits a

smooth radial decay with an e-fold length $\lambda_{I_{\text{sat}}}\sim 3\text{cm}$. When the antenna Q5 is powered, in the perturbed zone, the radial variation depends strongly on Z. Near $Z=0$, I_{sat} keeps its value without RF or even increases by 20% for $\delta r=-1\text{cm}$. Near the bottom of the antenna I_{sat} is reduced by 85%. This ‘current hole’ is radially centered near side limiters with the same radial extension than the potential peak (2cm) but contrary to V_{float} a stronger depletion is observed on the lower part of the antenna than on the upper part which is consistent with the up-down asymmetries of the heat deposition observed with the IR camera.

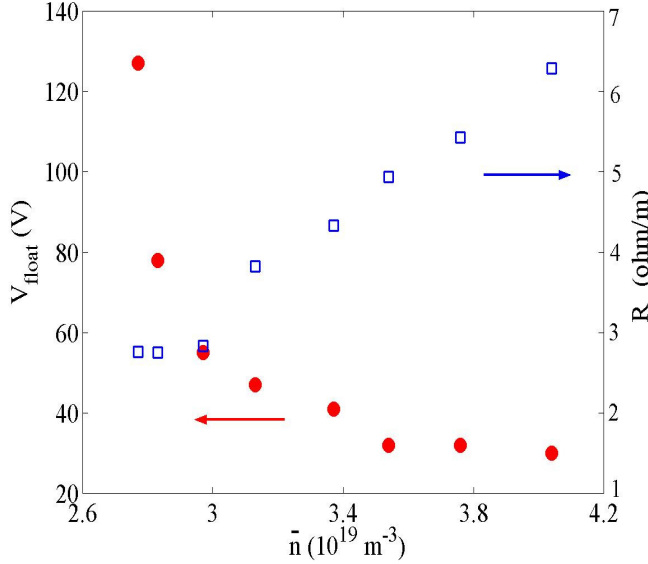


Figure 4. Maximum of V_{float} and coupling resistance as a function of the line-averaged density

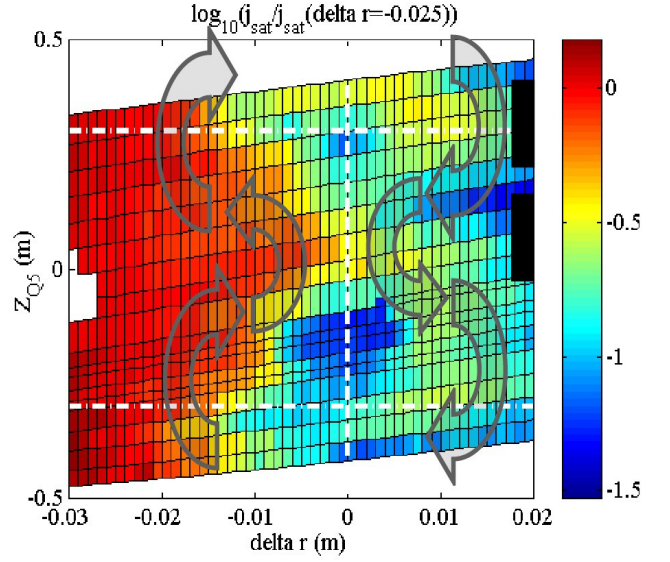


Figure 5. 2-D map of normalized $I_{\text{sat}}/I_{\text{sat}}(\delta=-0.025)$. Black boxes indicate connections to the lower and upper rows of C2 waveguides.

Density perturbation affects the coupling of the LHRF antennas when magnetically connected to the ICRF antenna. This is the case of the launcher C2 located in an adjacent port of the Q5 antenna ($\Delta\phi=40^\circ$). When the launcher is 2cm behind the ICRF antennas, starting from a balanced coupling with equal reflection coefficients (RC) for the upper and lower waveguide rows (RC=3%), the injection of 2MW by Q5 increases the RC of the lower rows to RC~5% and decreases the RC of the upper rows to RC~1%. Such a low RC indicates a strong local density modification and the 2-D map of I_{sat} (figure 5) indicates that the lower and upper waveguides are indeed connected to ‘cold’ (low density) and ‘hot’ (high density) flux tubes respectively. This increase of density has two main drawbacks: it enhances the fast electron production (see next section) and it favors the arcing at the waveguide aperture. When the initial RC is 5%, the lower waveguide RC can exceed 10% which can also limit the power handling. Similar interaction between close LHRF and ICRF antennas have been observed on JET [7].

V_{float} and T_e maps indicate a strong positive biasing of the plasma at the top and the bottom of the antenna which is related to the RF currents flowing in the antenna frame. A Faraday screen with small misalignment with respect of the field lines ($<3.5^\circ$) does not reduce the perturbation. $E\times B$ drift produced by ∇V_{float} may explain the strong modulation of the density (j_{sat}), as iso- j_{sat} curves on the 2D map of figure 5 have a shape similar to iso- V_{float} curves (sketched by the arrows). The resulting convective cells are consistent with the asymmetry of power deposition.

4. Plasma convection induced by fast electrons in the near field of LHRF antennas

In the near-field of LHRF launchers, thermal electrons can be accelerated by Landau damping up to ~ 2 keV [8]. Fast electrons intercept weakly the radiating waveguides when the toroidal radius of curvature of the antenna is properly matched to the field lines and the heat flux on the launcher guard limiters which acts as the main target does not exceed 3MW/m^2 for optimal coupling conditions. These fast electrons can also intercept the ICRF antenna guard limiters when this antenna is protruding with respect of the LHRF launcher. Hot spots due to this interaction is observed on the Q1 and Q5 antennas. The accelerated electrons escaping from the near-field give rise to a positive charge in front of the launcher which in turn produce a radial and poloidal electric field \mathbf{E} [9]. This radial electric field was accurately measured on the CASTOR tokamak with a hot emissive probe[10]. The main resulting $\mathbf{E} \times \mathbf{B}$ drift is directed upwards on Tore Supra and an up/down asymmetry of the particle flux (j_{sat}) and density is expected. This asymmetry was measured on the C3 launcher. Langmuir probe data (~ 60 shots) show that the inhomogeneity increases with the local launched LH power and, on average, $(j_{\text{sat}})_{\text{up}}/(j_{\text{sat}})_{\text{down}} \sim 2$ and $(n_e)_{\text{up}}/(n_e)_{\text{down}} \sim 1.5$ for $P=2.-2.5\text{MW}$. The data are indeed very scattered and the reason of this scattering is not fully understood but particle recycling is likely to play an important role. The resulting RC unbalance is quite moderate in contrast to the asymmetry due to ICRF-induced perturbation. IR images and visual inspection of the waveguides confirm this inhomogeneity of the power deposition on the waveguides. Figure 6 shows an IR image of the C3 launcher ($P=1.6\text{MW}$) in a case where strong density unbalance is measured. The IR image has been superimposed to a high resolution CCD image by a non-linear warping technique in order to localize precisely the power-deposition on the launcher. At a smaller scale, the bright spots appear in the upper part of the waveguides when no heating is detected on the lower part of the waveguides [11]. Modeling of a waveguide row by a two fluid code indicates that a density asymmetry by up to a factor 3 and radial heat flux directed to the waveguides on their upper part (figure 7). The predicted heat flux is relatively small ($\sim 0.05\text{MW/m}^2$). This $\mathbf{E} \times \mathbf{B}$ -flow is further confirmed by inverting the magnetic field direction: the flow is then inverted [6-11].

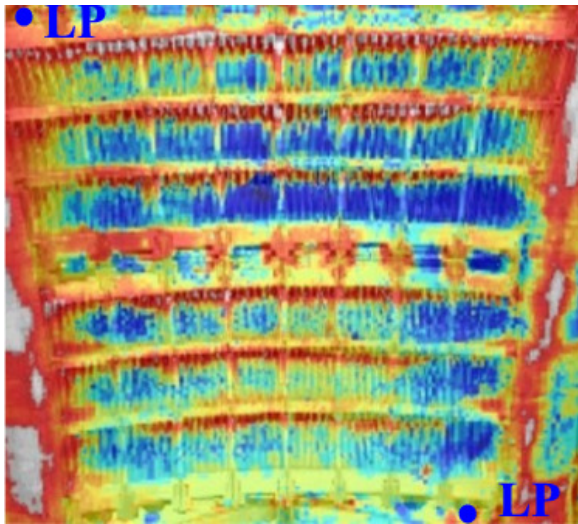


Figure 6. IR image of the C3 launcher ($P=1.6\text{MW}$). The highest temperature is indicated in white, the lowest in blue. Density of LP is $(n_e)_{\text{up}}/(n_e)_{\text{down}} = 1.6 / 0.6 \times 10^{18}\text{m}^{-3}$

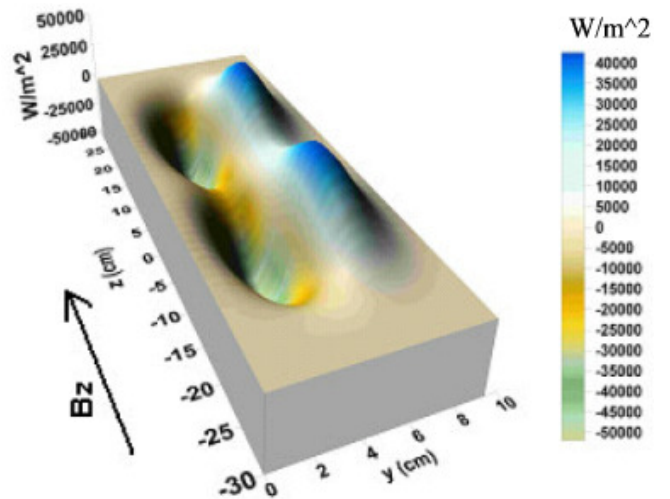


Figure 7. Modeling of the radial heat flux for a waveguide row (The flux is positive when directed onto the waveguides)

5. Fast ion losses and scaling of the power deposition on the RF antennas

An additional heat flux was found on all antennas during ICRF experiments. This heat flux is identified with no ambiguity on ICRF antennas when one antenna is not powered to avoid private power effects described previously. The location of the heat deposition moves from the lower left corner to the upper right corner when the magnetic field is reversed. Plasma density increase or hydrogen injection during the plasma shot decreases this specific heat flux. This heat flux is attributed to the loss of energetic ions by the drift of their banana orbits in the strong rippled magnetic field (5.5% at the LCFS), mainly caused by collisionless stochastic diffusion. An orbit following code indicates that only the most energetic ions ($E \geq 500\text{keV}$) can reach these components. These ions impinge on the lower part of the left side limiter which is the ion drift side on Tore Supra since the magnetic field has been reversed on Tore Supra. This is measured by the IR diagnostic and confirmed by calorimetric data indicating that a strong unbalance of the power loading on some (but not all) of the side limiters occurs during ICRF experiments. The fast ions reach also the shadowed radiating components (Faraday screen or waveguides). From simple Monte-Carlo simulations it is deduced that a parallel energy exceeding 350keV is required to have $\sim 10\%$ of the ions escaping the 10cm long side limiter and impinge on the Faraday screen or waveguides.

The temperature measured by IR on the C3 launcher lower left corner (figure 8) is well modeled by the 3D thermo-mechanical Cast3M code when a heat flux of 1MW/m^2 is included during ICRF power injection ($P_{\text{ICRF}}=4\text{MW}$, $\bar{n} = 2.7 \times 10^{19}\text{m}^{-3}$) and taking into account an emissivity $\varepsilon=0.4$ for the copper-alloy waveguides [12]. A similar heat flux was estimated on the ICRF Faraday screens for similar conditions. For this launcher, the temperature increase of the lower left corner with respect of the upper left corner is plotted as a function of the ICRH power (figure 9).

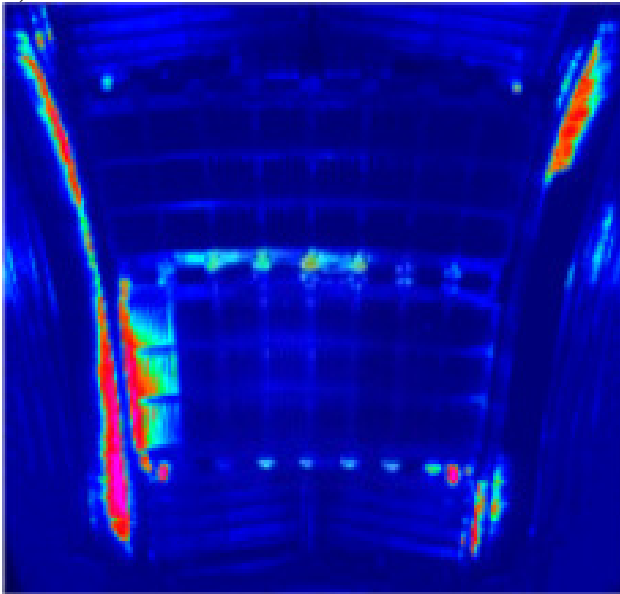


Figure 8. IR image of C3 launcher during ICRF injection ($P_{\text{ICRF}}=5.5\text{MW}$).

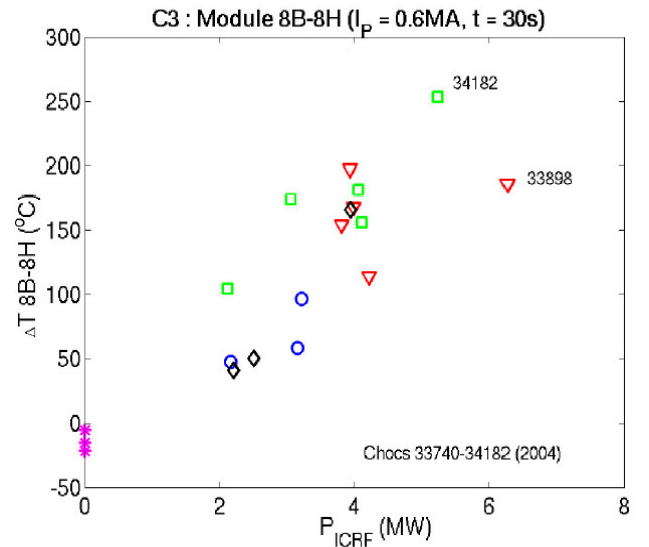


Figure 9. Relative increase of temperature of the C3 left corner as a function of P_{ICRF} for a 20s P_{ICRF} duration. The different densities are indicated by different symbols.

From the calorimetric data, a scaling of the energy extracted by the antennas ($E_{\text{extracted}}$) is computed. Three sources were considered, the RF losses (LHRF) or the sheath-induced losses (ICRF), the convected/ conducted power from thermal particles (P_{th}) and the fast ion losses. The scaling reads as $E_{\text{extracted}} = k_1 E_{\text{ant}} + k_2 (E_{\text{tot}} - E_{\text{rad}}) + k_3 E_{\text{ICRF}}$ where E_{ant} is the energy injected by the

studied antenna, E_{tot} is the total injected energy, E_{rad} the total radiated energy and E_{ICRF} , the injected ICRF energy. Normalizations are performed to take into account specific scalings which are here pre-scribed: RC for LHRF losses, power and density dependence ($P^{1/2}n$) for sheath-induced losses, antenna positions in the SOL for the convected/conducted power, slowing-down time τ_{SD} for the fast ion losses. For this last dependence $\tau_{\text{SD}} \sim T_e^{3/2}/n_e n_H$, a constant n_H/n_D is assumed. On Tore Supra, H concentration varies between ~ 3 and ~ 7 % for most of the experiments and the uncertainty of this measurement is too large to take into account this parameter. Experiments of the database were performed at two plasma currents (0.6 and 0.9MA), with LHRF power varying between 0 and 4.5 MW, ICRF power between 0 and 8.5 MW, total injected energy between 50 and 1070MJ. For the C3 launcher, the scaling is established on a 72 shot basis with equal numbers of ICRF-heated shots performed at $I_p=0.6\text{MA}$ and $I_p=0.9\text{MA}$. The following parameters are found for the scaling $k_1=4.35\%$, $k_2=0.85\%$ and $k_3=1.15\%$ (figure 9). RF losses are just slightly higher than expected from calculation ($\sim 3\%$). This could be the result of the deleterious effect of the connected ICRF antenna on coupling. The scaling for the $I_p=0.6\text{MA}$ and 0.9MA pulses are very similar and no direct effect of the plasma current on the fast ion losses can be detected. A similar result was found for the fast ions lost by ripple trapping and diffusing in the ∇B direction [13]. However, the 0.9MA series is performed, in average, at higher density ($\langle \bar{n} \rangle = 3.8 \times 10^{19} \text{m}^{-3}$ vs $2.8 \times 10^{19} \text{m}^{-3}$) and consequently, without normalization of slowing-down time, the ion losses are clearly lower by 32% (0.85 % vs 1.25%). The robustness of this scaling was verified by selecting only the 43 pulses with $E_{\text{C3}}/E_{\text{tot}} < 0.3$ in order to reduce the weight of the RF losses, the k_3 factor is then reduced by 14% whereas k_2 factor increases by 9% and k_1 is unchanged.

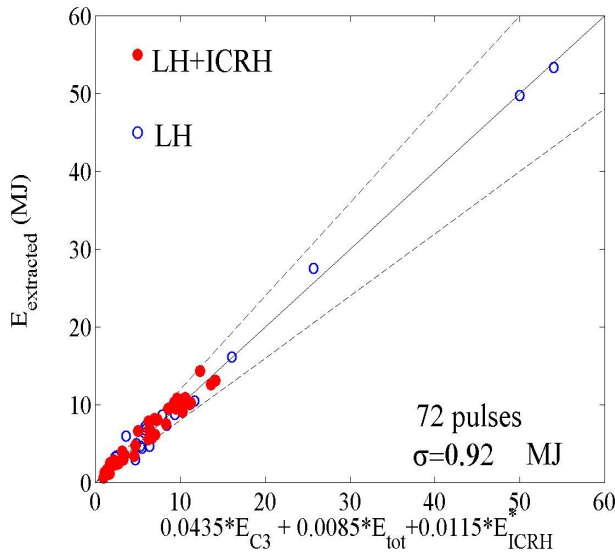


Figure 10. Scaling of the energy extracted by the C3 launcher

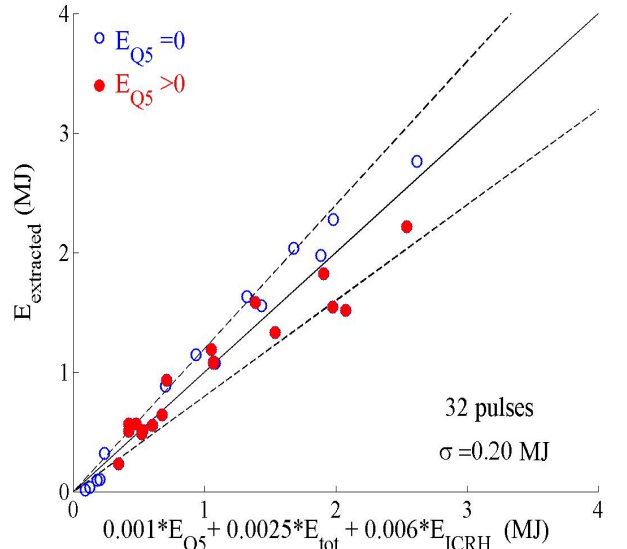


Figure 11. . Scaling of the energy extracted by the Q5 antenna.

For ICRF antennas Faraday screen, the same analysis is performed from a more reduced number of pulses (24). For a launched power of 1MW, the sheath-induced losses (k_1) is estimated to be only 0.1%. Due to the larger gap between the limiter and the screen when compared to LHRF antennas, the convected/conducted power (k_2) accounts for 0.25%. The fast ion losses ($k_3=0.6\%$) is also smaller. There is no clear reason why the fast ion losses are smaller for the ICRF antenna. Similar parameters, within $\pm 0.1\%$, are found for the other ICRF antennas. More generally, estimation of the power extracted by the 5 antennas and their limiters indicates strong toroidal

asymmetries which cannot be fully explained by geometrical effects (shadowing). Total ion losses is estimated to be in the range of 6-8 % of the total ICRF power for $T_e(0)=5\text{keV}$ and $\bar{n}=3.3\times 10^{19}\text{m}^{-3}$.

The calorimetric data were confronted to the IR measurements. With 9MW of injected power (5.5MW of ICRF power), the C3 scaling gives a power flux from the plasma (including radiation) $P_{\text{rad}}+P_{\text{th}}=0.15\text{ MW/m}^2$. The very small increase of temperature of the antenna surface not exposed to the fast ion bombardment is consistent with this value. According to the IR images, it can be assumed that 6% of the total surface of the antenna interacts with the fast ions. A flux of 2.5 MW/m^2 is then deduced from the scaling which is close to the value inferred from IR and Cast3M code (2 MW/m^2). Sheath-induced losses lead to a peak value of the flux of $\sim 1\text{MW/m}^2$ for a coupled ICRF power of 1MW.

6. Conclusions and perspectives

Different sources of plasma interaction with RF antennas has been identified. For ICRF antennas, sheath effects can lead to high localized heat flux specially on the antenna box corners which need to be carefully designed. A new electric scheme, proposed for ITER and soon tested on Tore Supra, will be the opportunity to test the theoretical models. The strong poloidal inhomogeneity of density on a radial width of $\sim 2\text{cm}$ may have deleterious effects on connected LHCF launchers. However, it is not clear why on Tore Supra the C3 antenna is less perturbed than the C2 launcher and further investigations are needed for assessing rules for the ITER antennas location. The fast ion losses require specific 3D codes with the full geometry of the antennas and limiters to explain the observed toroidal anisotropy. Such a code is being developed. On ITER, the ferromagnetic inserts will reduce the magnetic ripple to a low value (0.7%) which will reduce the fast ion losses to a level more easy to handle.

The identification of these different sources of have been crucial for the development of the real-time power control on Tore Supra [14,15]. This has allowed to optimize the RF power output, while minimizing deleterious effects and 9.5MW have been recently injected for 23s with controlled temperature excursion of the five antennas and their limiters. The different scalings of the antenna power loading can be used for the design of the ITER RF antennas.

References

- [1] D.Guilhem et al., *Fusion Engineering and Design* **74** (2005) 879-883
- [2] L.Colas, S.Heurax, S.Br mond, G.Bosia, *Nucl. Fusion* **45** (2005) 767-782
- [3] V. Petr ilka & al., proc. EPS conf. Plasma Phys. Tarragona 2005, ECA Vol.**29C**, P-2.095
- [4] L.Colas et al., 17th Plasma Surface Interactions conference, P3-4, 22-26 May 2006, Hefei Anhui, China (2006)
- [5] M. B coulet, L. Colas, S. P coul et al., *Plasma Physics* **9**, 2619 (2002)].
- [6] L.Colas et al., *Nucl. Fusion* **46** (2006) S500-S513
- [7] A.Ekedahl et al., Proc. of the 15th Top.Conf.on RF Power in Plasmas, AIP, **694** (2003) 259
- [8] M.Goniche et al., *Nuclear Fusion*, **28** (1998) 919-937
- [9] V. Petr ilka et al., 30th EPS Conference on Contr. Fusion and Plasma Phys., St. Petersburg, 7-11 July 2003 ECA Vol. **27A**, P-1.195
- [10] F.Zacek, Petr ilka and M.Goniche, *Plasma Phys.Control.Fusion*, **47** (2005) L17
- [11] A.Ekedahl, 17th Plasma Surface Interactions conference, O-8, 22-26 May 2006, Hefei Anhui, China (2006)
- [12] C.Portafaix et al., 24th Symposium on Fusion Technology, Warsaw, Poland, September 2006, Thermal behavior of the LHCD launchers in Tore Supra, P3-B-109
- [13] V.Basiuk, *Nucl. Fusion* **44** No 1 (January 2004) 181-192
- [14] Ph.Moreau et al., 24th Symposium on Fusion Technology, Warsaw, Poland, September 2006, Thermal behavior of the LHCD launchers in Tore Supra, P2-C-197
- [15] E.Joffrin et al., 21st IAEA Fusion Energy Conference, Chengdu, China, 16-21 Oct.2006, EX/1-6